PHYSICAL REVIEW E **92**, 012505 (2015)

Reexamination of the mean-field phase diagram of biaxial nematic liquid crystals: Insights from Monte Carlo studies

B. Kamala Latha,[*] Regina Jose, K. P. N. Murthy, and V. S. S. Sastry
School of Physics, University of Hyderabad, Hyderabad 500046, Telangana, India

(Received 6 November 2014; published 15 July 2015)

Investigations of the phase diagram of biaxial liquid-crystal systems through analyses of general Hamiltonian models within the simplifications of mean-field theory (MFT), as well as by computer simulations based on microscopic models, are directed toward an appreciation of the role of the underlying molecular-level interactions to facilitate its spontaneous condensation into a nematic phase with biaxial symmetry. Continuing experimental challenges in realizing such a system unambiguously, despite encouraging predictions from MFT, for example, are requiring more versatile simulational methodologies capable of providing insights into possible hindering barriers within the system, typically gleaned through its free-energy dependences on relevant observables as the system is driven through the transitions. The recent paper from this group [Kamala Latha *et al.*, Phys. Rev. E **89**, 050501(R) (2014)], summarizing the outcome of detailed Monte Carlo simulations carried out employing an entropic sampling technique, suggested a qualitative modification of the MFT phase diagram as the Hamiltonian is asymptotically driven toward the so-called partly repulsive regions. It was argued that the degree of (cross) coupling between the uniaxial and biaxial tensor components of neighboring molecules plays a crucial role in facilitating a ready condensation of the biaxial phase, suggesting that this could be a plausible factor in explaining the experimental difficulties. In this paper, we elaborate this point further, providing additional evidence from curious variations of free-energy profiles with respect to the relevant orientational order parameters, at different temperatures bracketing the phase transitions.

DOI: 10.1103/PhysRevE.92.012505 PACS number(s): 64.70.mf

I. INTRODUCTION

The thermotropic biaxial nematic phase, which was predicted by Freiser [1] nearly four decades ago, has attracted considerable attention recently for various reasons, ranging from a fundamental question of conducive experimental conditions for its realization, to its envisaged applications in display devices. Even though predictions made by various mean-field (MF) theoretic treatments [2–9], Landau free-energy-based analyses [10–14], and computer simulations [15–22] support the feasibility of such a phase, success on the experimental front has been rather modest [23]. Experimentally, the biaxial phase was first obtained in a lyotropic, ternary mixture of potassium laurate, 1-Decanol, and D_2O in 1980 [24] and more recently in bent-core compounds [25,26], organo-siloxane tetrapodes [27,28], LC polymers [29], and colloidal systems of Goethite particles [30]. Though recent experiments [31,32] point to low transition enthalpies for rod-disk systems, an unambiguous biaxial phase has not been established in such systems. From the point of view of application, it is anticipated that the minor director could switch more readily compared to the major director in an external field [20,33], leading to faster response times. Even in the recent case of bent-core molecules, there appears to be a debate on the consistency in the experimental findings [34–37]. Achieving spontaneous macroscopic biaxiality in nematic liquid crystal phases with appreciable biaxial order appears at the moment to be a challenge.

Recent theoretical studies, on the other hand, point to a more optimistic picture: they predict that the condensation of a biaxial phase could occur over a wide range of the Hamiltonian parameter space of a general quadrupolar model [5–9]. However, the analysis of the mean-field model was noted to be unsatisfactory, as the phase behavior of the biaxial system in the limit of vanishing intermolecular biaxial interaction traversing in the process the so-called partly repulsive region of the Hamiltonian was found to be contravening the biaxial phase stability criterion [9]. In this context, we revisit the mean-field phase diagram with detailed Monte Carlo simulations. The main results of this study were briefly presented recently [38]. The other MC work on the so-called μ model [39] was also similarly concerned with the consequences of the contribution of a repulsive interaction term in the Hamiltonian.

In this paper, we present the details of a qualitatively different type of Monte Carlo sampling that we adopted for the study. It was observed that the sampling methods to extract equilibrium averages based on equilibrium ensembles (constructed using the METROPOLIS algorithm [40]) largely lead to results in agreement with the mean-field theory (MFT) in the so-called attractive region of the Hamiltonian parameter space. Keeping this in view, we adopted the Wang-Landau sampling procedure [41] augmented by frontier sampling [42,43] to determine the representative density of states of the system, enabling the calculation of all relevant thermodynamic properties. We find that this more versatile and efficient technique results in qualitatively different results in certain regions of the parameter space, leading to the proposal of a modified phase diagram (relative to MFT). We argue that such differences, which develop progressively as the "partly repulsive region" is reached, are important in understanding the relative roles of different contributions to the intermolecular tensor interactions.

The mean-field Hamiltonian model employed and its representation for purposes of simulation are outlined in Sec. II. The

---

[*] Corresponding author: kklata@gmail.com

©2015 American Physical Society

sampling technique and the simulation details are presented in Sec. III. The observations based on these computations are presented in Sec. IV, followed by conclusions in Sec. V.

II. HAMILTONIAN MODEL

The MF analysis [5–9] is based on the general quadrupolar orientational Hamiltonian, proposed by Straley [2] and set in terms of tensors [5]. Accordingly, the interacting biaxial molecules are represented by two pairs of symmetric, traceless tensors ($\boldsymbol{q}$, $\boldsymbol{b}$) and ($\boldsymbol{q}'$, $\boldsymbol{b}'$). Here $\boldsymbol{q}$ and $\boldsymbol{q}'$ are uniaxial components about the unit molecular vectors $\boldsymbol{m}$ and $\boldsymbol{m}'$, whereas $\boldsymbol{b}$ and $\boldsymbol{b}'$ (orthogonal to $\boldsymbol{q}$ and $\boldsymbol{q}'$, respectively) are biaxial. These irreducible components of the anisotropic parts of the susceptibility tensor are represented in its eigenframe $(\boldsymbol{e},\boldsymbol{e}_\perp,\boldsymbol{m})$ as

$$\boldsymbol{q} := \boldsymbol{m}\otimes\boldsymbol{m} - \frac{\boldsymbol{I}}{3}, \tag{1a}$$

$$\boldsymbol{b} := \boldsymbol{e}\otimes\boldsymbol{e} - \boldsymbol{e}_\perp\otimes\boldsymbol{e}_\perp, \tag{1b}$$

where $\boldsymbol{I}$ is the identity tensor. Similar representations hold for $\boldsymbol{q}'$ and $\boldsymbol{b}'$ in the eigenframe $(\boldsymbol{e}',\boldsymbol{e}'_\perp,\boldsymbol{m}')$. The interaction energy is written as

$$H = -U[\xi\,\boldsymbol{q}\cdot\boldsymbol{q}' + \gamma(\boldsymbol{q}\cdot\boldsymbol{b}' + \boldsymbol{q}'\cdot\boldsymbol{b}) + \lambda\,\boldsymbol{b}\cdot\boldsymbol{b}'], \tag{2}$$

where U is the scale of energy, $\xi = \pm 1$, and γ and λ are dimensionless interaction parameters, determining the relative importance of the uniaxial-biaxial coupling and biaxial-biaxial coupling interactions between the molecules, respectively.

Mean-field analysis of the Hamiltonian identifies a triangular region OIV in the (γ,λ) plane—called the essential triangle—representing the domain of stability into which any physical system represented by Eq. (2) can be mapped [7,9] (see Fig. 1). The dispersion parabola $\lambda = \gamma^2$ [4] traverses through the interior of the triangle, intersecting IV at point T, called the Landau point. The region of the triangle above the parabola corresponds to a Hamiltonian where all the terms are attractive, while the region below is noted to be partly repulsive [7]. In particular, a mean-field (MF) phase diagram was predicted [9] as a function of the arc length OIV (Fig. 1), denoted by λ^*, defined as $\lambda^* = \lambda$ on the segment OI, and

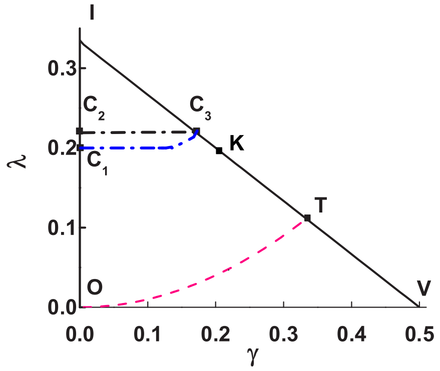

FIG. 1. (Color online) Essential triangle: Region of biaxial stability. OI and IV are uniaxial torque lines intersecting at point I (0,1/3). OT is the dispersion parabola, which meets the line IV at the Landau point T. Point V (1/2,0) is the limit of biaxial stability for the interaction. C_1 (0,0.2) and C_3 (5/29,19/87) are tricritical points, and C_2 (0.22,0) is a triple point [9]. K (0.2,0.2) is a point where $\mu = -1$ (refer to the text).

$$\lambda^* = \frac{(1+\sqrt{13}\gamma)}{3},$$

with

$$\gamma = \frac{(1-3\lambda)}{2}$$

covering the segment IV. The MF phase diagram predicts for $\lambda^* \lesssim 0.22$ ($\gamma = 0$, $\lambda \lesssim 0.22$) a two-stage transition from an isotropic to a biaxial phase, with an intervening uniaxial nematic phase. The uniaxial-biaxial transition is computed to be second order ($N_B = N_U - I$) up to the point C_1 ($\gamma = 0,\lambda \simeq 0.2$), and then it changes to first order ($N_B - N_U - I$) until C_2 ($\gamma = 0,\lambda \simeq 0.22$). For the rest of the range of λ^*, a direct isotropic-biaxial transition is expected, extending up to V in Fig. 1. This transition is predicted to be first order ($N_B - I$) for $\lambda^* \leqslant 0.54$, ($C_3,\lambda^* = 0.54,(\gamma = 5/29,\lambda = 19/87)$) and second order ($N_B = I$) up to the point V ($\gamma = 0.5,\lambda = 0.0$). Hence C_1 and C_3 are tricritical points and C_2 is a triple point.

We consider here the diagonal form of the interaction Hamiltonian in Eq. (2) [7,9] expanded as a superposition of two quadratic terms, i.e.,

$$H = -U(a^+\boldsymbol{q}^+\cdot\boldsymbol{q}^{+'} + a^-\boldsymbol{q}^-\cdot\boldsymbol{q}^{-'}),$$

where $\boldsymbol{q}^+$ and $\boldsymbol{q}^-$ are orthogonal molecular biaxial tensors represented as

$$\boldsymbol{q}^\pm = \boldsymbol{q} + \gamma^\pm\boldsymbol{b}$$

with

$$\gamma^\pm = \frac{3\lambda - 1 \pm \sqrt{(3\lambda-1)^2 + 12\gamma^2}}{6\gamma}, \quad a^+ = \frac{\gamma^- - \gamma}{\gamma^- - \gamma^+},$$

and

$$a^- = \frac{\gamma - \gamma^+}{\gamma^- - \gamma^+}.$$

Along OI, where $\gamma = 0$, $\boldsymbol{q}^+ = \boldsymbol{q}$, $\boldsymbol{q}^- = \boldsymbol{b}$, $a^+ = 1$, and $a^- = \lambda$, implying that $\boldsymbol{q}^+$ is pure uniaxial and $\boldsymbol{q}^-$ is pure biaxial and the Hamiltonian reduces to an interaction in terms of a single parameter λ,

$$H = -U(\boldsymbol{q}\cdot\boldsymbol{q}' + \lambda\boldsymbol{b}\cdot\boldsymbol{b}'). \tag{3}$$

Similarly, along IV, defined by $1 - 3\lambda - 2\gamma = 0$, the Hamiltonian is expressed in terms of uniaxial tensor $\boldsymbol{q}_2^*$ and biaxial tensor $\boldsymbol{b}_2^*$ as [9]

$$H = -U\frac{1-\lambda}{2}(-\mu\,\boldsymbol{q}_2^*\cdot\boldsymbol{q}_2^{*\prime} + \boldsymbol{b}_2^*\cdot\boldsymbol{b}_2^{*\prime}), \tag{4}$$

where

$$\boldsymbol{q}_2^* = -\frac{1}{2}\boldsymbol{q}^- = \left(\boldsymbol{e}\otimes\boldsymbol{e} - \frac{\boldsymbol{I}}{3}\right),$$

$$\boldsymbol{b}_2^* = \frac{3}{2}\boldsymbol{q}^+ = (\boldsymbol{m}\otimes\boldsymbol{m} - \boldsymbol{e}_\perp\otimes\boldsymbol{e}_\perp),$$

and

$$\mu = \frac{(1-9\lambda)}{(1-\lambda)}.$$

The pairwise interaction in Eq. (4) now reduces to

$$H = U'\left[\mu\left(\boldsymbol{e}\otimes\boldsymbol{e}-\frac{\boldsymbol{I}}{3}\right)\cdot\left(\boldsymbol{e}'\otimes\boldsymbol{e}'-\frac{\boldsymbol{I}}{3}\right)\right.$$
$$\left.-(\boldsymbol{e}_\perp\otimes\boldsymbol{e}_\perp-\boldsymbol{m}\otimes\boldsymbol{m})\cdot(\boldsymbol{e}'_\perp\otimes\boldsymbol{e}'_\perp-\boldsymbol{m}'\otimes\boldsymbol{m}')\right] \quad (5)$$

with $U' = U(1-\lambda)/2$. In this format, $\mu = -3$ corresponds to the point I (0, 1/3) in Fig. 1, $\mu = 0$ to the Landau point T (1/3,1/9) (LP), and $\mu = +1$ to V (0.5, 0.0). In particular, we observe that $\mu = -1$ corresponds to $\lambda^* \simeq 0.57$ located at K (0.2,0.2) in Fig. 1.

For simulation purposes, the general Hamiltonian in Eq. (2) is conveniently recast as a biaxial mesogenic lattice model, where particles of D_{2h} symmetry, represented by unit vectors $\boldsymbol{u}_a,\boldsymbol{v}_b$ on lattice sites a and b, interact through a nearest-neighbor pair potential [44]

$$U = -\epsilon\{G_{33} - 2\gamma(G_{11}-G_{22}) + \lambda[2(G_{11}+G_{22}) - G_{33}]\}. \quad (6)$$

Here $f_{ab} = (\boldsymbol{v}_a\cdot\boldsymbol{u}_b)$ and $G_{ab} = P_2(f_{ab})$, with P_2 denoting the second Legendre polynomial. The constant ϵ (set to unity in simulations) is a positive quantity setting the reduced temperature $T' = k_BT/\epsilon$, where T is the absolute temperature of the system. This is recast along IV of the triangle, using Eq. (17) in Ref. [39], in terms of the parameter μ as

$$H = \epsilon[\mu G_{11} + (-2G_{33} - 2G_{22} + G_{11})]. \quad (7)$$

III. DETAILS OF THE SIMULATION

The Wang-Landau (WL) sampling [41] is a flat histogram technique designed to overcome energy barriers encountered, for example, near first-order transitions, by facilitating a uniform random walk along the energy (E) axis through an appropriate algorithmic guidance. The sampling, originally developed for Hamiltonian models involving random walks in discrete configurational space, continues to be applied to various problems in statistical physics [45,46] and polymer and protein studies [47–49], and it is being developed for more robust applications for continuous systems [50–56] and self-assembly [57]. The proposed algorithm was modified [58] to suit lattice models such as the Lebwohl-Lasher interaction [59], allowing for continuous variation of molecular orientations. It was subsequently augmented with the so-called *frontier* sampling technique [42,43] to simulate more complex systems such as the biaxial medium. The WL sampling is based on effecting a convergence of an initial distribution over energy E to the density of states (DOS) $g(E)$ of the system iteratively. The frontier sampling technique is an algorithmic guidance, provided in addition to the WL routine, by which the system is constrained to visit and sample from low entropic regions. The modified Wang-Landau algorithm using entropic sampling augmented by frontier sampling [43] is described below.

We consider a cubic lattice (size: $L \times L \times L, L = 15,20$) with each lattice site representing a biaxial molecule, and hence hosting a (right-handed) triad of unit vectors. We initiate the process by assigning random orientations of all the axes at every site, and we compute the energy of the system at the chosen point in the (γ,λ) plane with the Hamiltonian in Eq. (6) [corresponding to $\xi = 1$ in Eq. (2)], under periodic boundary conditions. The temperature is thus measured in reduced units. The energy range of interest of the system $(E_{\min},E_{\max})$ is divided into N bins (we set $N = 40\ L^3$) of equal width, and the bin energies are indexed as E_i, corresponding to the values at the center of the ith bin. We indexed these bins starting from $E_{\min}$. We initialize $g(E_i)$ to an array $g^{(0)}(E_i)$ with equal values $(i = 1,\ldots,N)$, where the superscript is the iteration run index and the subscript is the energy bin index. The estimate of $g(E_i)$ is improved by updating iteratively, until it converges to the density of states within a set tolerance limit.

For liquid crystal systems with continuous degrees of freedom for the random walk in configuration space, we find it necessary to perform the simulations on a log-log scale to avoid issues of large numbers and consequent overflow problems. Following [60], we work with $\zeta_i = \log(\alpha_i) = \log\{\log[g(E_i)]\}$, where α_i represents the microcanonical entropy. The acceptance criterion as well as reweighting procedures are implemented on this scale.

During the random walk, the system is permitted to transit from an initial configuration with an instantaneous value ζ_i to a trial configuration with ζ_t with a probability given by

$$p = \min\boldsymbol{\{}1, \exp\boldsymbol{[} - \exp(\zeta_t + \log\{1-\exp[-(\zeta_t-\zeta_c)]\})\boldsymbol{]\}}. \quad (8)$$

We update the values of ζ_i $(i = 1,\ldots,N)$ of the bins with a Gaussian centered at the accepted bin energy value (say E_0), as

$$\zeta_i \rightarrow \zeta_i + \gamma_0 \exp\left(\frac{-(E_i-E_0)}{\delta}\right)^2. \quad (9)$$

Here (γ_0,δ) represent the modification parameters. We kept δ constant through the simulation (at $0.002 \times N$) and chose the initial value of $\gamma = 0.1$. The random walk of the system over the energy bins, at this value of γ_0, is carried out for a large number of lattice sweeps (attempted L^3 moves), typically 10^7 sweeps or more depending on the system size. The γ_0 value is reduced to $\gamma_0 \rightarrow 0.95\gamma_0$, and the procedure is repeated until γ_0 reaches a set small value close to zero (10^{-4}). The computations involving a progressive reduction of γ_0, starting from the initial high value to the set low value, constitute an iteration. After two such successive iterations, the differences between histogram values at each bin are determined. If the differences are nearly uniform over some energy range, it implies that this region is adequately sampled. We expect, on entropic grounds, that the flatness of the distribution, in terms of fairly uniform increments of histogram values, is achieved more readily starting from the maximum energy value. We refer to the limiting lower energy bin, satisfying the flatness criterion, as the *frontier*, say E_c. Following the suggestion of [42], we update the values of the histogram above E_c by a uniform value (say, 0.5). This causes the system, under the above acceptance criterion, to perform a random walk preferentially in the lower-energy region hosting less accessible states, until the histogram values build up to match the values in the higher-energy regions, above E_c. This process is continued with such iterations, and new frontiers are identified at progressively lower energy values, corresponding

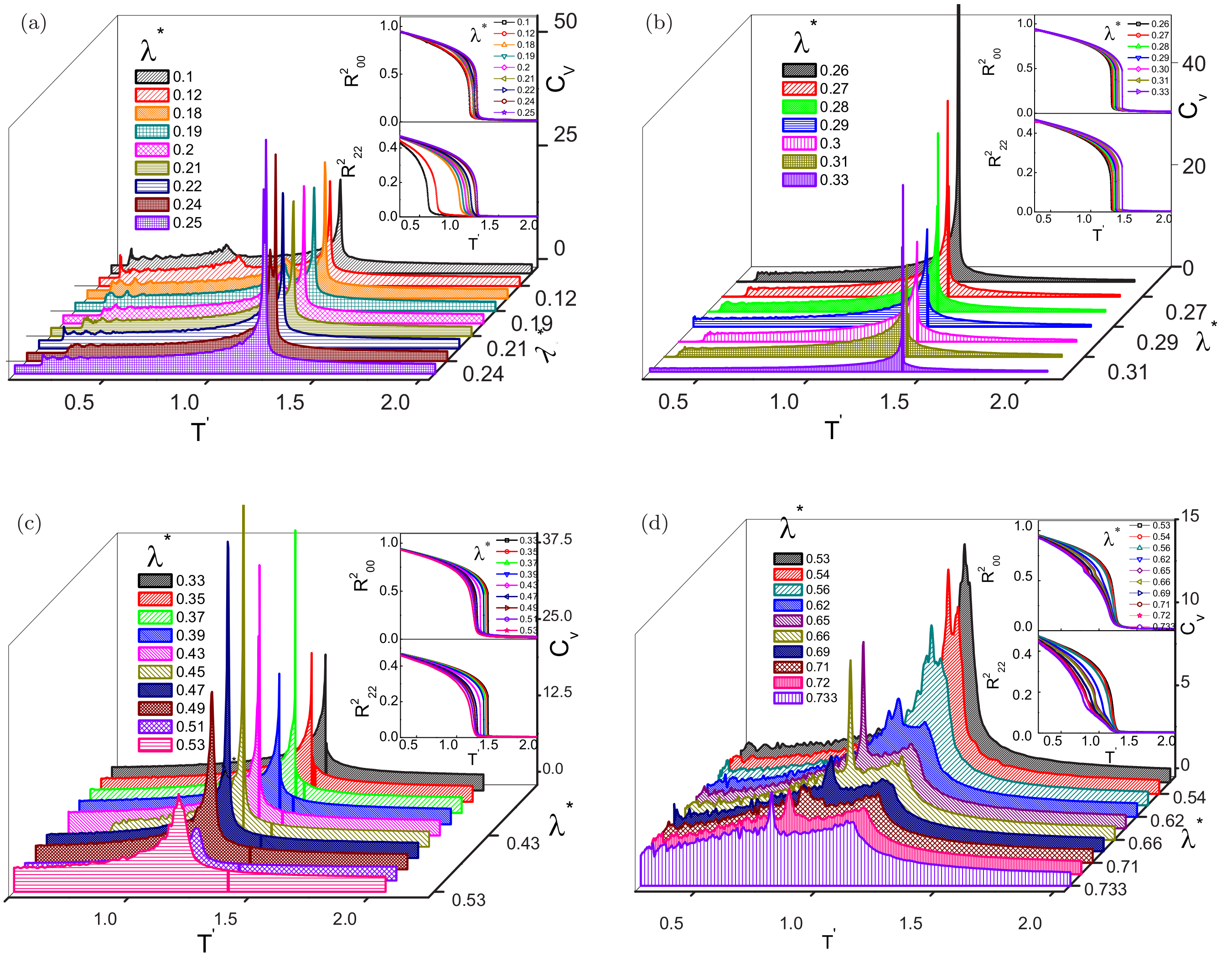

FIG. 2. (Color online) Temperature variation of the specific heat (in arbitrary units) for different ranges of λ*: (a) 0.1–0.25, (b) 0.26–0.33, (c) 0.33–0.53, and (d) 0.53–0.733. Corresponding variations of the two primary order parameters (R^2_{00} and R^2_{22}) are shown in the insets with the same color scheme. Splitting of the C_v peaks in (d) for $\lambda^* > 0.53$ and qualitative changes in the temperature variation of order parameters are clearly observed.

to an approximate estimation of the DOS over larger energy ranges, until the frontier reaches $E_{\min}$.

Consequently, a long smoothing run is performed (no frontiers are identified at this stage) starting with initial values of (γ_0,δ) set to $(0.001,\ 0.002 \times N)$, and the value of γ_0 is progressively decreased during this computation until it reaches practically zero value, $\simeq 10^{-9}$. Such iterations continue until a specified flatness criterion is met over the entire energy range. This ensures that the final $\zeta(E_i)$ converges to its asymptotic value and is representative of the density of states of the system, within the tolerances prescribed by the flatness criterion.

We now construct a large entropic ensemble of microstates (say, $M \sim 4 \times 10^7$) by effecting a random walk of the system over the energy bins $(i = 1,\ldots,N)$ with an acceptance probability based on $g^{-1}(E_i)$ [analogous to Eq. (8)]. We label the microstates as C^i_ν $[i = 1,\ldots,N, \nu = 1,\ldots,M]$ with $M \gg N$. We note that an ith bin, for example, hosts a large number of microstates (C^i_ν) with distinct energies $E(C^i_\nu)$, however it is represented by the same density of states $g(E_i)$.

The relevant thermodynamic quantities are calculated at each temperature by constructing an appropriate canonical ensemble of states using a reweighting technique [61]. We refer to these ensembles as RW ensembles to differentiate from those constructed through the METROPOLIS guided random walk (B ensembles). The equilibrium averages of a physical variable "O" at a temperature T ($\beta = \frac{1}{k_B T}$) are computed through this procedure as

$$\langle O \rangle = \frac{\sum_{C^i_\nu} O\big(C^i_\nu\big) g(E_i) \exp\big[-\beta E\big(C^i_\nu\big)\big]}{\sum_{C^i_\nu} g(E_i) \exp\big[-\beta E\big(C^i_\nu\big)\big]}. \tag{10}$$

The representative free energy F, as a function of the energy of the system, as well as of the two dominant order parameters (uniaxial and biaxial orders), is computed from the DOS and the microcanonical energy, both of which are available as a function of bin number in the entropic ensemble.

The WL simulations were carried out at different values of (γ,λ) in Eq. (6) so as to trace the trajectory OIV of the essential triangle in Fig. 1 at about 60 chosen points.

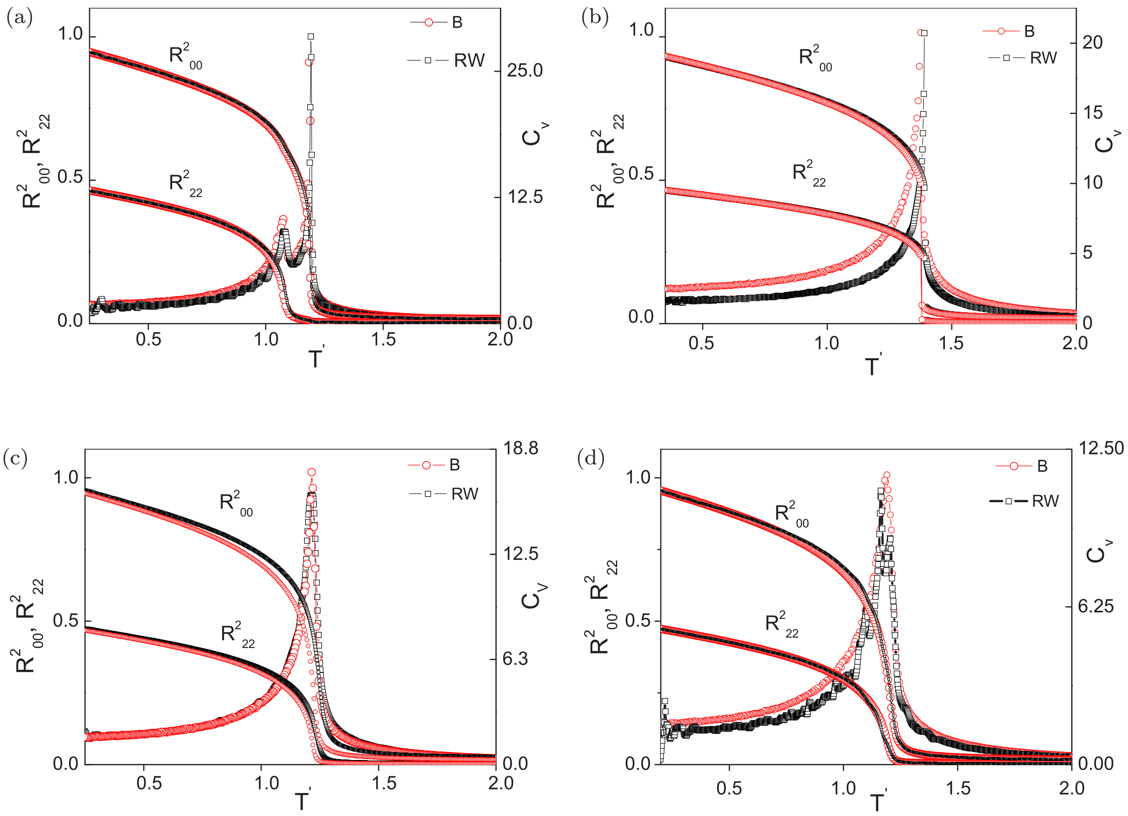

FIG. 3. (Color online) Comparison of the results obtained from B ensembles (hollow red circles) and RW ensembles (hollow black squares): Temperature variation of the specific heat (in arbitrary units) and corresponding variations of the two primary order parameters (R^2_{00} and R^2_{22}) are shown for different values of λ^* in regions OI and IV: (a) 0.2, (b) 0.33, (c) 0.51, and (d) 0.54. The overlap of the corresponding curves [(a)–(c)] clearly indicates the agreement between the two ensembles up to $\lambda^* = 0.53$ as mentioned in the text. Part (d) shows the qualitative disagreement first noticed at $\lambda^* = 0.54$.

For purposes of comparison, conventional MC sampling (based on the METROPOLIS algorithm) was used to construct canonical (Boltzmann) ensembles. Considering an attempted $N = L^3$ moves as one lattice sweep (MC step), the system is equilibrated, and a production run is carried out, each for 6×10^5 MC steps. In our analysis, we find it necessary to distinguish between the averages from B ensembles and RW ensembles.

The physical parameters of interest in this system, calculated at each λ^*, are the average energy $\langle E\rangle$, specific heat C_v, energy cumulant V_4 [$= 1 - \langle E^4\rangle/(3\langle E^2\rangle^2)$], which is a measure of the kurtosis [62], the four order parameters of the phase calculated according to [17,63], and their susceptibilities. These are the uniaxial order $\langle R^2_{00}\rangle$ (along the primary director), the phase biaxiality $\langle R^2_{20}\rangle$, the molecular contribution to the biaxiality of the medium $\langle R^2_{22}\rangle$, and the contribution to uniaxial order from the molecular minor axes $\langle R^2_{02}\rangle$.

The averages are computed at a temperature resolution of 0.002 units in the temperature range [0.05, 2.05]. The temperature T' of the simulation is scaled to conform to the values used in the mean-field treatment: $1/\beta^* = 3T'/\{9[2U(1+3\lambda)]\}$ [7,9]. Statistical errors in different observables are estimated over ensembles comprising a minimum of 5×10^5 microstates, and these are compared with several such equilibrium ensembles at the same (γ,λ) value, but initiating the random walk from different arbitrary points in the configuration space. We find that the relative errors in energies are 1 in 10^5, while those in the estimation of the order parameters are 1 in 10^4. We also note that these error estimates from RW ensembles are smaller relative to B ensembles of comparable size by at least an order of magnitude, due to the efficacy of the importance sampling involved in the reweighting procedure.

IV. RESULTS

The temperature variations of the specific heat and the two dominant scalar order parameter (R^2_{00} and R^2_{22}) values obtained from RW ensembles at various values of λ^* along the arc OIT (λ^* axis) are shown in Figs. 2(a)–2(d).

It is noted from Fig. 2(a) that for all values of λ^* in the range 0.1–0.25, two transition peaks are observed in the specific heat. As the biaxial system is cooled from the high-temperature isotropic phase, an initial $I - N_U$ transition occurs at a high temperature, T_1, followed by a second transition $N_U - N_B$ at lower temperature, T_2. The $I - N_U$ transition temperature remains fairly constant with the variation in λ^*, whereas the $N_U - N_B$ transition shifts toward higher temperatures as λ^* increases from 0.1 to 0.25. This behavior is also reflected in the order-parameter profiles shown in the inset. The two transitions eventually coalesce at $\lambda^* = 0.26$, resulting in a triple point, and a direct isotropic-biaxial ($I - N_B$) transition occurs from

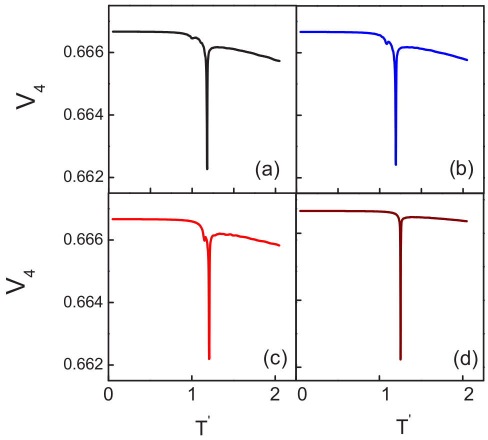

FIG. 4. (Color online) Variation of energy cumulant with temperature, at different λ^* values: (a) 0.18, (b) 0.2, (c) 0.22, and (d) 0.26.

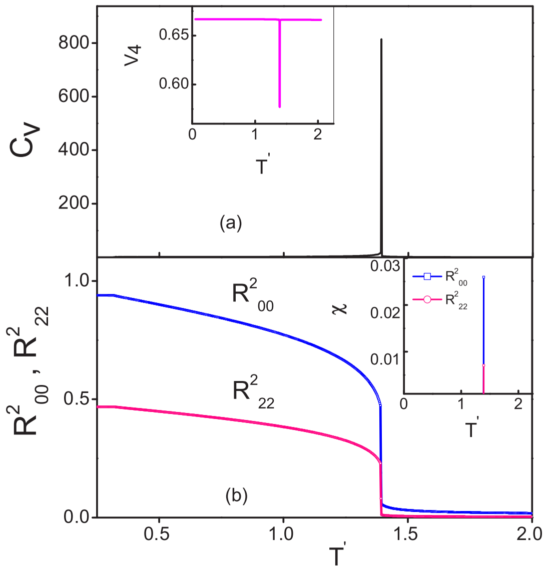

FIG. 5. (Color online) (a) Specific-heat profile with (inset) energy cumulant; (b) order parameters with (inset) susceptibility profiles for $\lambda^* = 0.33$. Point I of the essential triangle is the intersection point of the three uniaxial torque axes [9] and hosts the strongest first order $I - N_B$ transition, as shown by the very sharp features of these physical properties.

$\lambda^* = 0.26$ to 0.53, as depicted by the specific-heat profiles and order parameters (inset) of Figs. 2(b) and 2(c). These results from RW ensembles agree qualitatively with those obtained from the B ensembles in the range of $\lambda^* = 0.1$–0.53.

A comparative study of the WL and MC simulation results for certain representative values of λ^* are shown in Figs. 3(a)–3(d). It is observed that qualitative agreement with the mean-field predictions exists up to $\lambda^* \leqslant 0.53$, and deviations of the RW ensembles from MF and B ensembles start from $\lambda^* = 0.54$ $(5/29,19/87)$ (i.e., C_3 in the essential triangle of Fig. 1).

Referring to Fig. 2(a), the results from RW ensembles agree with MF predictions except for the actual values of the location of the tricritical and triple points C_1 and C_2. In this respect, one has to make allowances for unavoidable finite-size effects on the simulation data on the one hand, and the inherent approximate nature of the mean-field theoretical analysis in this respect on the other.

At $L = 20$, the simulation results show that the tricritical point lies in the neighborhood of $\lambda^* = 0.18$; the nature of the $N_U - N_B$ transition appears to change to (weak) first order for values of $\lambda^* \geqslant 0.18$, as evidenced from the energy cumulant data shown in Fig. 4. The triple point is located at $\lambda^* \sim 0.26$ (the corresponding MF value is $\sim$0.22) as the transition sequence $I - N_U - N_B$ changes to $I - N_B$ at this value of λ^* [see Fig. 2(b)]. Transition temperatures derived from these simulations are summarized in Table I.

It is of interest to observe that the $I - N_B$ transition progressively becomes very strongly first order as the λ^* value increases to $1/3$ and is most pronounced at the point corresponding to coordinates $(0,1/3)$ (Fig. 1). Figure 5 depicts the specific heat with (inset) energy cumulant and order parameters with (inset) their susceptibilities for this value of λ^*.

This feature of the transition is also demonstrated by the variation of the representative free energy obtained from

TABLE I. Transition temperatures in the range of $\lambda^* = (0.18,0.26)$: T_1' and T_2' are transition temperatures (in reduced units) obtained from simulation, while T_1^* and T_2^* are the corresponding equivalent mean-field temperatures.

λ^*	T_1'	T_2'	T_1^*	T_2^*
0.18	1.1753	0.9919	0.1272	0.1074
0.2	1.1937	1.0770	0.1243	0.1122
0.22	1.2110	1.1490	0.1216	0.1153
0.26	1.2516		0.1172	

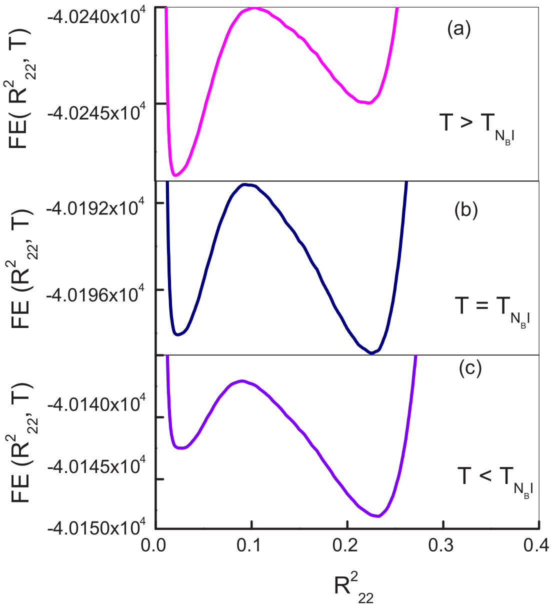

FIG. 6. (Color online) Representative free energy (in arbitrary units) as a function of biaxial order parameter R_{22}^2 at (a) $T > T_{N_B I}$, (b) $T = T_{N_B I}$, and (c) $T < T_{N_B I}$ at $\lambda^* = 0.33$ for a system of size $L = 15$.

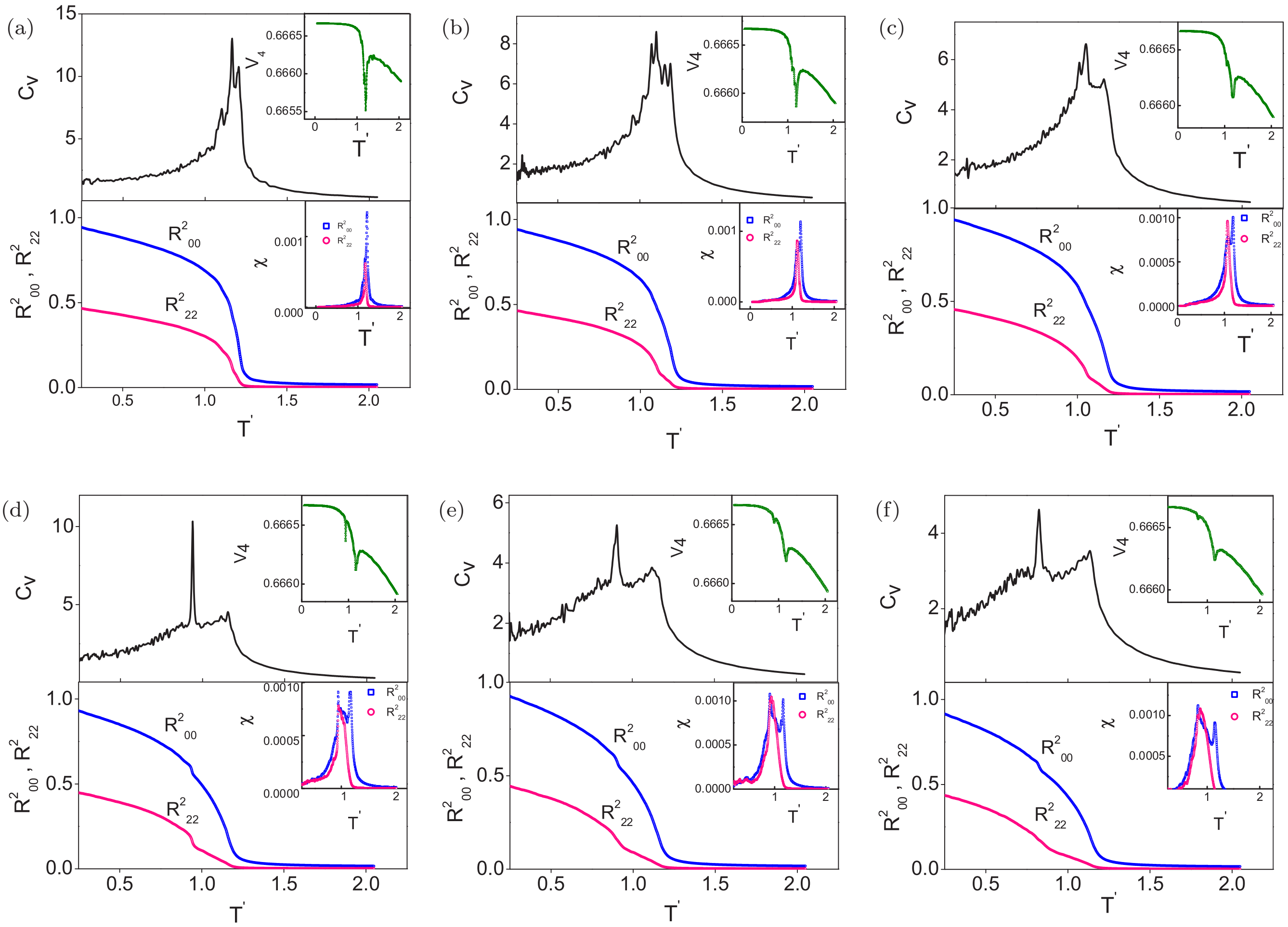

FIG. 7. (Color online) Specific-heat profile with (inset) energy cumulant V_4 and order parameters with (inset) susceptibility profiles at different λ^* values (a) 0.54, (b) 0.58, (c) 0.62, (d) 0.66, (e) 0.69, and (f) 0.72.

the DOS and bin energies, as a function of the two order parameters. As an example, we depict its variations across the transition ($\lambda^* = 0.330$, $L = 15$) in Fig. 6. Observation of such a strong free-energy barrier (see the coexistence region at $T = T_{N_B I}$) is supportive of the MF prediction at I. Very similar plots result as a function of R^2_{00} also.

Referring to Fig. 2(d), we observe that the C_v peak splits starting from $\lambda^* \sim 0.54$, signaling the onset of two transitions. The temperature gap between transition peaks increases with λ^* above this value, attaining a maximum at $\lambda^* = 0.733$ (T on the triangle). These observations are illustrated in Fig. 7, plotting all the relevant variables as a function of temperature at chosen values of λ^* (0.54, 0.58, 0.62, 0.66, 0.69, and 0.72) along the segment C_3T. These graphs depict the temperature variation of specific heat C_v with energy cumulant V_4 (inset) and order parameter (R^2_{00}, R^2_{22}) profiles along with respective susceptibilities χ (inset).

The nature of the two phases below the clearing point is inferred from the order-parameter profiles and their susceptibility peaks. Referring to the two transition temperatures in decreasing order as T_1 and T_2, the data indicate that the onset of a biaxial phase takes place at T_1 itself, and the growth of biaxial order in the intermediate phase is marginal as compared to the uniaxial order. Furthermore, both the uniaxial and biaxial order parameters display a sudden upward jump at T_2, and subsequently increase rapidly (more pointedly the biaxial order R^2_{22}) as the temperature is lowered further. This behavior is prominent in the neighborhood of $\lambda^* = 0.66$. The susceptibility of R^2_{00} exhibits two peaks corresponding to the two transitions, whereas that of R^2_{22} shows only a single peak at T_2 for all values of λ^*. The energy cumulant V_4 shown in the inset of each of the figures indicates the first-order nature of the $I - N_{B1}$ transition (at T_1). The additional second dip at the lower-temperature transition (at T_2) appears to point toward the progression of the first-order nature of the $N_{B1} - N_B$ transition. It is observed that the dip in the cumulant at T_2 is maximum at $\lambda^* = 0.66$.

We also examined the representative free energy plotted as a function of the order parameters at the transition temperatures T_1 and T_2. These variations observed near T_1, for different λ^* values (covering the region C_3T), are shown in Fig. 8. Focusing on Figs. 8(a) and 8(b), one immediately observes that both free-energy profiles (with respect to R^2_{00} and R^2_{22}) at T_1 show a distinctive indication of a developing minimum at a lower temperature evidenced by the systematic deviations (from a smooth continuation) of the profiles at the respective

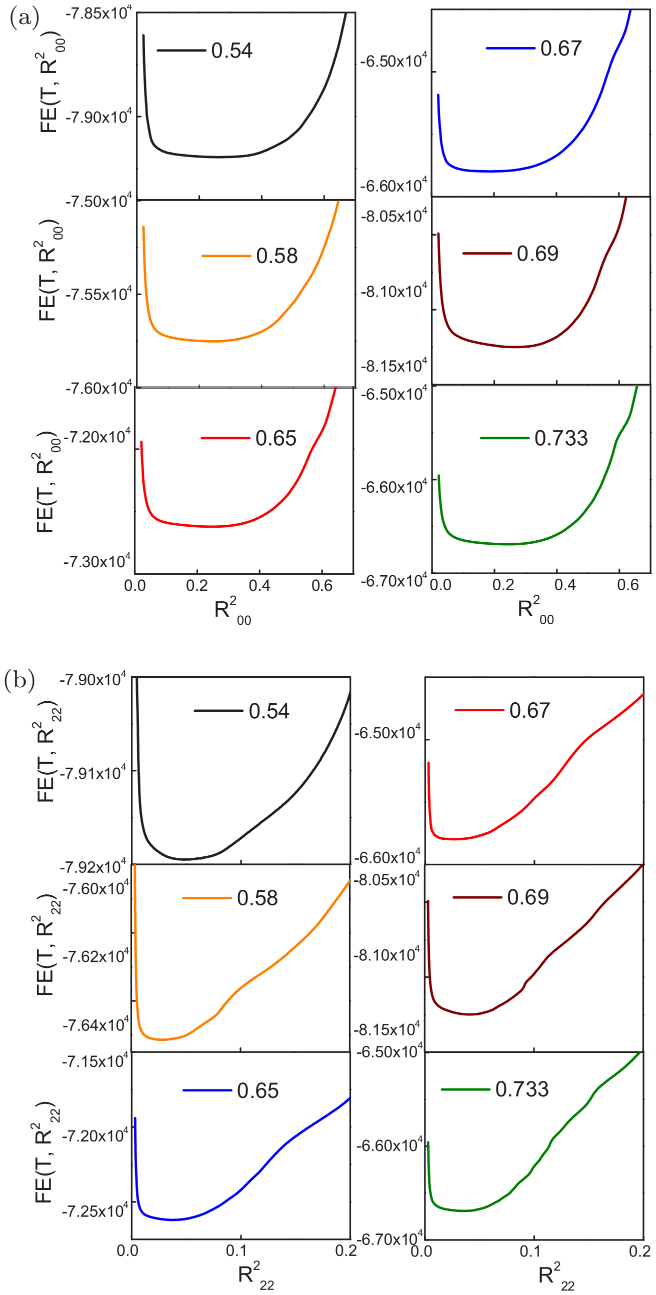

FIG. 8. (Color online) Free energy shown as a function of (a) R^2_{00} and (b) R^2_{22}, at the transition temperature T_1 for λ^* values in the region C_3T of Fig. 1.

higher values of the two order parameters. And, as λ^* increases in the C_3T region, the location of these sharp deviations shifts progressively to a higher value of the corresponding order parameter.

We tracked the variation of these profiles closely from T_1 to T_2 (shown in Fig. 9 for a single value of $\lambda^* = 0.65$), and we found that the free-energy minima gradually shift toward high-order regions, and the second transition at T_2 corresponds to a gradual shift of the free-energy minima toward the curious regions, depicted in Fig. 8. The variation of the free energy at T_2 is shown in Figs. 10(a) and 10(b) for different values of λ^* (in region C_3T). These depict a free-energy minimum attained at T_2 for all values of λ^*.

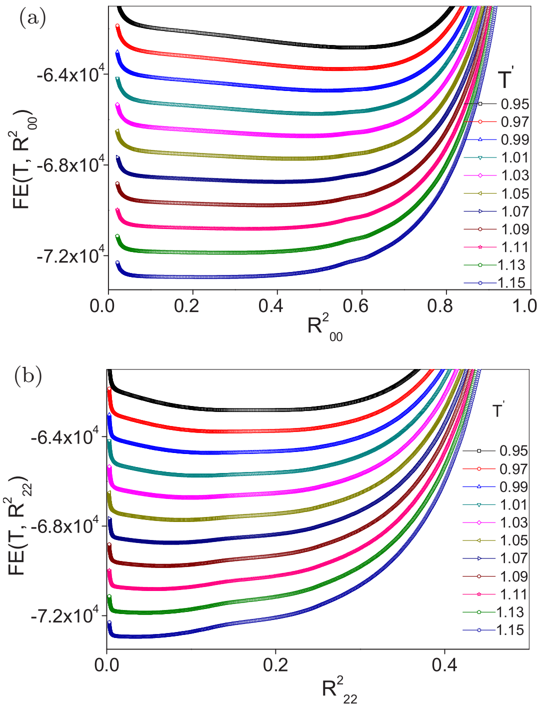

FIG. 9. (Color online) Free energy shown as a function of (a) R^2_{00} and (b) R^2_{22}, on cooling from T_1 to T_2 for $\lambda^* = 0.65$.

We argue that the progression of the free-energy profiles with temperature, as a function of R^2_{00} and R^2_{22}, and matching of the values of respective order parameters at T_2 with the location of sharp deviations observed in Fig. 8, are further evidence for the existence of two transitions in this region. This could be made possible only by adopting a MC sampling procedure that facilitates the computation of free-energy profiles of the system via the density of states.

We are thus led to the conclusion that in this region of λ^* values, the medium undergoes two transitions, and both low-temperature phases have biaxial symmetry. From the data on the limited temperature region available for the intermediate phase, and in comparison with the low-temperature phase, it appears that the biaxial order in the intermediate phase is somewhat inhibited, presumably by free-energy barriers. It is only after the second transition at T_2 (between the two biaxial phases, and hence necessarily a first-order transition) that the biaxial order shows a normal increase with a decrease in temperature, as is to be expected. Thus we propose the phase sequence in this region to be $N_B - N_{B1} - I$.

We now construct the phase diagram as a function of the arc length λ^* based on the specific-heat data (from RW ensembles), shown in Fig. 11 at 56 values of λ^* distributed over the arc OIV (see [38] for details). The transition temperatures at a few representative values of λ^* beyond the Landau point T (segment TV) are obtained from the B ensemble data. The temperature T' of the simulation is scaled to conform to the values $1/\beta^*$ used in the mean-field treatment as discussed in Sec. III.

A comparison of the phase diagram proposed from the current MC simulations [38] with that predicted based on mean-field theory [9] brings out clear qualitative differences in

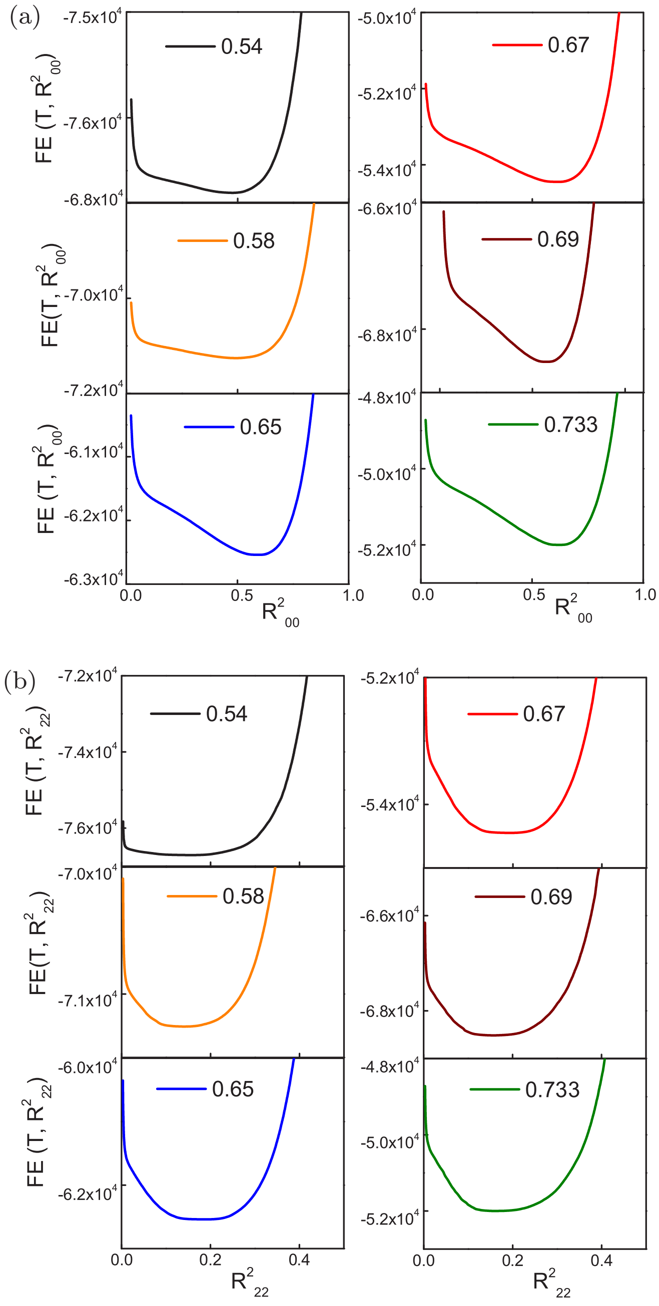

FIG. 10. (Color online) Free energy shown as a function of (a) R^2_{00} and (b) R^2_{22}, at the transition temperature T_2 for λ^* values in the region C_3T of Fig. 1.

the region C_3TV of the essential triangle. We observe that the predicted direct transition from the isotropic to biaxial phase is replaced by two transitions in which an intermediate biaxial phase occurs between these two phases. These results begin to deviate starting from $\lambda^* \gtrsim 0.54$, very close to point C_3 in Fig. 1. The fact that B ensembles constructed from simple configurational random walks based on the METROPOLIS algorithm fail to detect the second transition in this λ^* region merits some discussion.

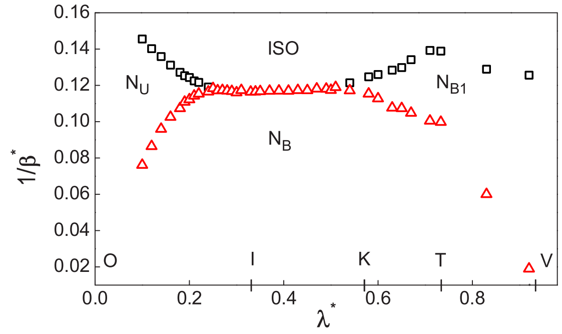

FIG. 11. (Color online) Phase diagram as a function of λ^*, derived from RW ensembles. The transition temperature $1/\beta^*$ is scaled to conform to mean-field values as indicated in the text. Points along OIV in Fig. 1 are mapped onto the λ^* axis for reference. An additional biaxial-biaxial transition is observed in the region KTV in place of a single transition (to the biaxial phase) predicted by the mean-field theory [38].

V. DISCUSSION

To look for the origin of the additional low-temperature specific-heat peak observed in the region C_3T, which was not detected by Boltzmann sampling, we made a comparison of the simulation results from RW ensembles with those obtained from B ensembles at $\lambda^* = 0.733$ (1/3,1/9) (Landau point T) shown in Fig. 12. The location of T is unique as it is the intersection point of the dispersion parabola with segment IV. MF theory predicts a direct transition from the isotropic to biaxial phase at this point, and it is the only such

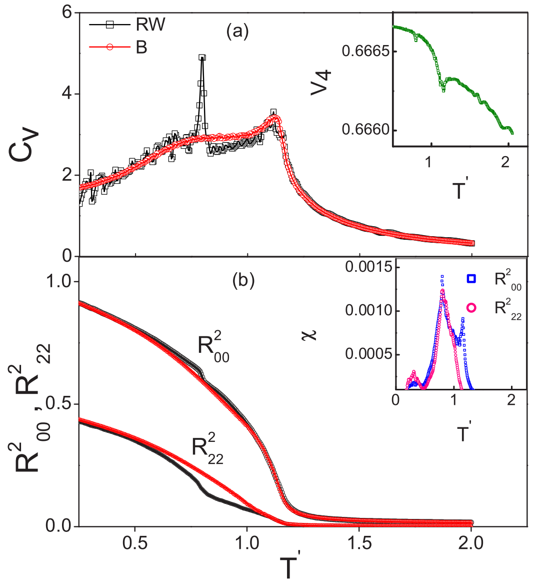

FIG. 12. (Color online) Comparison of data, as a function of temperature, from the B and RW ensembles, at the Landau point T (1/3,1/9): (a) Specific heat C_v and (b) order parameters R^2_{00} and R^2_{22}. The insets focus on (a) the energy cumulant V_4 and (b) order parameter susceptibilities (χ's), both derived from RW ensembles ($\lambda^* = 0.733$).

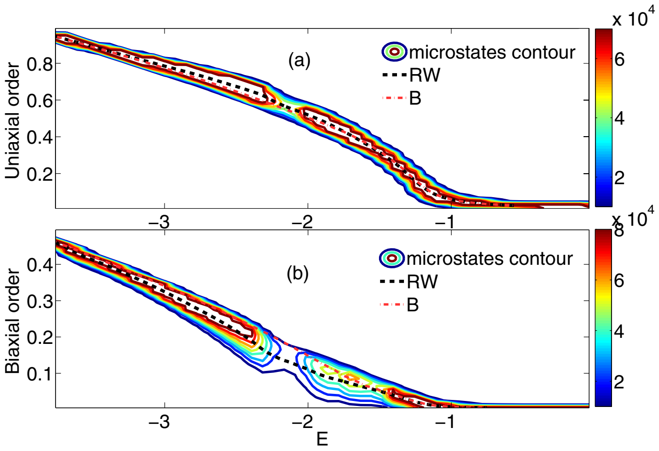

FIG. 13. (Color online) Contour plots of the distribution of microstates collected in the entropic ensemble at $\lambda^* \simeq 0.733$: (a) microstate energy vs its uniaxial order and (b) microstate energy vs its biaxial order. The superimposed red (dash-dotted line) and black (dashed) lines are thermal averages from B and RW ensembles, respectively.

point on the parabola. From the perspective of the interaction Hamiltonian, the coordinates (γ,λ) of T represent a unique symmetry: The Hamiltonian has no interaction between the uniaxial components of the molecular tensor [$\mu = 0$ at T; see Eq. (5)], and it is purely biaxial in nature (involving $\boldsymbol{m}$ and $\boldsymbol{e}_\perp$ axes). A consequence of the present findings in this context is curious. They do confirm the presence of a direct transition from the isotropic to biaxial symmetry, but these also indicate that there is yet another biaxial-to-biaxial transition at a lower temperature. Further, the onset of the first biaxial phase at T_1 does not lead to a natural progression of the biaxial order with a decrease in temperature, and it is only after the transition at T_2 that the macroscopically significant and hence observable R^2_{22} value seems to be realizable.

We thus focus on the Landau point, and we present the simulation results obtained from the two types of MC sampling methods: data from B ensembles and from RW ensembles. Figure 12 shows the specific heat (energy cumulant as inset) and order parameters (susceptibilities as inset), computed as a function of temperature at point T, obtained from these ensembles. It should be noted that the derived physical variables from B ensembles do not betray the onset of the second transition at T_2, thus lending support to MF predictions, as has been noted in the earlier report on this work [38].

We now examine the contour maps of the distribution of microstates in the entropic ensemble (set of microstates that are approximately uniformly distributed with respect to energy) collected at the Landau point. Figure 13(a) depicts such a contour map in the space of uniaxial order and energy (per site), along with the thermal averages computed from RW ensembles and B ensembles superposed for ready comparison. Similarly, Fig. 13(b) shows a corresponding contour map plotted between biaxial order and energy (per site), along with thermal averages of the two canonical ensembles again superposed. The traversal path of the B-ensemble averages is seen to be encompassing regions corresponding to contour peak positions, whereas the RW-ensemble average is observed to follow a different trajectory, consequent to encompassing a wider collection of microstates visiting sparse regions, corresponding to large deviations of the order parameter. This is seen as a manifestation of the process of collection of microstates of the entropic ensemble by the algorithm employed, representative in their distribution (with respect to energy) of the underlying density of states. As has been pointed out and argued earlier (Fig. 6 in [38]), the algorithmic guidance of the WL procedure is seeking out all accessible microstates (an approximate microcanonical ensemble) in each bin of energies, in the process visiting relatively rare states that correspond to larger excursions in the order parameter, and hence correspondingly larger fluctuations of the component energies of the Hamiltonian in Eq. (6), while conforming to the same energy bin. The requirement of an accurate determination of DOS through the entropic sampling procedure apparently demands inclusion of these rare microstates, and the process of reweighting used to construct the equilibrium ensembles through this elaborate procedure includes them in the thermal averages as a consequence.

Thus the differences observed in the averages from the two procedures are to be appreciated from the standpoint of simulations. As has been discussed [38], these rare microstates indeed correspond to situations in which the ordering of either of the molecular axes (involved in the D_{4h} symmetry of the pairwise interaction, i.e., $\boldsymbol{m}$ or $\boldsymbol{e}_\perp$) form a spontaneous and equally probable calamitic axis during the evolution of the system, by virtue of having the largest instantaneous eigenvalue of the diagonalized ordering tensors of the three molecular axes. It is apparent that conventional sampling methods, not under algorithmic compulsion to estimate the DOS of the system, are not geared to sample such rare states, and hence they come up with different averages. In the process, it appears that the second low-temperature transition is not evident in the earlier work.

In addition, we note that the deviation of the simulation results from the mean-field expectations occurs along the diagonal IV of the essential triangle where the pairwise interaction Hamiltonian has D_{4h} symmetry and is expressed in reduced form as in Eq. (5) in terms of a single parameter μ. It is observed that the deviations start from $\lambda^* \geqslant 0.54$ [point C_3 (5/29,19/87)] and continue until the Landau point where $\mu = 0$. It should be noted that point K (0.2,0.2) corresponding to $\mu = -1$ is very close to point C_3 (0.172,0.218). It can be inferred from Eq. (7) that, starting from the neighborhood of K, the uniaxial attractive coupling of the $\boldsymbol{e}$ axis becomes lower in strength than that of the (biaxial) attractive coupling of the other two axes, and it continues to decrease as λ^* increases on the diagonal. As a result, the ordering of the biaxially coupled $\boldsymbol{e}_\perp$ and $\boldsymbol{m}$ axes is favored as temperature is decreased, leading to the first onset of biaxial symmetry from the isotropic phase. This is followed by an ordering of the $\boldsymbol{e}$ axes at a lower temperature, leading to the stabilization of both orders, in particular biaxial order. Thus it appears that the growth of biaxial order in the intermediate biaxial phase is inhibited by the lack of long-range order of the $\boldsymbol{e}$ axes (in this region of the λ^* axis). As one approaches the Landau point, μ in Eq. (5) tends to zero (from the negative side), thereby suppressing the second transition temperature as well as weakening the efficacy of this term to drive a transition. This lack of concomitant ordering of all the molecular axes leads to inhomogeneity in the medium, and we tend to attribute all the interesting aspects of the simulation to this feature of the Hamiltonian.

Finally, we wish to comment on the curious role played by the WL algorithm in the analysis of the phase diagram. It has been already established that this algorithm assists the system in overcoming energy barriers of the system, as the simulation pushes the system to make a random walk in the configuration space, which is uniform with respect to energy. A successful convergence of the probability density yields a limiting distribution of microstates with respect to the total energy of the system—the representative density of states. The role of this algorithm in the present study seems to be qualitatively different and yet illustrative of its varied applicability. The WL algorithm, even while operating within a single energy bin (an approximate microcanonical ensemble), appears to seek out rare states, corresponding to the otherwise inaccessible fluctuations of the component energies, making up the total energy (see Fig. 6 in [38]). Inclusion of these microstates (as representative states for purposes of computing averages) is naturally embedded in the WL method while estimating the DOS accurately. We argue that the METROPOLIS sampling fails to access these states due to apparent energy barriers within the system inhibiting sampling of microstates with such large fluctuations in their energy components. We conclude that the results reported here are the outcome of this facet of efficiency of the entropic sampling.

VI. CONCLUSIONS

In conclusion, we present compelling evidence from Monte Carlo simulations based on entropic sampling to propose an additional biaxial phase along a region of the arc of the essential triangle, augmenting our earlier report [38]. The arguments advanced in this respect, particularly of the inevitable presence of inhomogeneities in the absence of a long-range order of the third stabilizing axis $\boldsymbol{e}$, seem to lend support to the findings (based on Boltzmann MC sampling) reported in the partly repulsive region of the λ^* axis (segment TV: the μ model [39]). At a more general level, we conclude that the cross-coupling between the uniaxial and biaxial tensor components of the neighboring molecules [γ term in Eq. (6)] seems to be playing an important role in determining the phase sequences. Furthermore, we suggest that its significant presence, even along trajectories inside the triangle (which could be relevant for practical purposes), should have such an inhibitive influence on the condensation of a biaxial phase with measurable biaxial order. Our recent simulational work on two such trajectories interior to the triangle are supportive of this conjuncture.

ACKNOWLEDGMENTS

We thank N. V. Madhusudana (Raman Research Institute, Bangalore, India) for useful discussions. B.K.L. acknowledges the grant of a research fellowship from the University Grants Commission, India during the tenure of this work. The simulations were carried out in the Centre for Modelling Simulation and Design, at the University of Hyderabad, India.

[1] M. J. Freiser, Phys. Rev. Lett. **24**, 1041 (1970).
[2] J. P. Straley, Phys. Rev. A **10**, 1881 (1974).
[3] D. K. Remler and A. D. J. Haymet, J. Phys. Chem. **90**, 5426 (1986).
[4] G. R. Luckhurst, C. Zannoni, P. L. Nordio, and U. Segre, Mol. Phys. **30**, 1345 (1975).
[5] A. M. Sonnet, E. G. Virga, and G. E. Durand, Phys. Rev. E **67**, 061701 (2003).
[6] G. De Matteis and E. G. Virga, Phys. Rev. E **71**, 061703 (2005).
[7] F. Bisi, E. G. Virga, E. C. Gartland, Jr., G. De Matteis, A. M. Sonnet, and G. E. Durand, Phys. Rev. E **73**, 051709 (2006).
[8] F. Bisi, S. Romano, and E. G. Virga, Phys. Rev. E **75**, 041705 (2007)
[9] G. De Matteis, F. Bisi, and E. G. Virga, Contin. Mech. Thermodyn. **19**, 1 (2007).
[10] R. Alben, Phys. Rev. Lett. **30**, 778 (1973).
[11] N. Bocara, R. Mejdani, and L. De Seze, J. Phys. (Paris) **38**, 149 (1977).
[12] E. F. Gramsbergen, L. Longa, and W. H. de Jeu, Phys. Rep. **135**, 195 (1986).
[13] D. Allender and L. Longa, Phys. Rev. E **78**, 011704 (2008).
[14] P. K. Mukherjee and K. Sen, J. Chem. Phys. **130**, 141101 (2009).
[15] G. R. Luckhurst and S. Romano, Mol. Phys. **40**, 129 (1980).
[16] M. P. Allen, Liq. Cryst. **8**, 499 (1990).
[17] F. Biscarini, C. Chiccoli, P. Pasini, F. Semeria, and C. Zannoni, Phys. Rev. Lett. **75**, 1803 (1995).
[18] C. Chiccoli, P. Pasini, F. Semeria, and C. Zannoni, Int. J. Mod. Phys. C **10**, 469 (1999).
[19] R. Berardi and C. Zannoni, Mol. Cryst. Liq. Cryst. **396**, 177 (2003).
[20] R. Berardi, L. Muccioli, S. Orlandi, M. Ricci, and C. Zannoni, J. Phys.: Condens. Matter **20**, 463101 (2008).
[21] G. De Matteis, S. Romano, and E. G. Virga, Phys. Rev. E **72**, 041706 (2005).
[22] G. Sai Preeti, K. P. N. Murthy, V. S. S. Sastry, C. Chiccoli, P. Pasini, R. Berardi, and C. Zannoni, Soft Matter **7**, 11483 (2011).
[23] G. R. Luckhurst, Nature (London) **430**, 413 (2004).
[24] L. J. Yu and A. Saupe, Phys. Rev. Lett. **45**, 1000 (1980).
[25] B. R. Acharya, A. Primak, and S. Kumar, Phys. Rev. Lett. **92**, 145506 (2004).
[26] L. A. Madsen, T. J. Dingemans, M. Nakata, and E. T. Samulski, Phys. Rev. Lett. **92**, 145505 (2004).
[27] K. Merkel, A. Kocot, J. K. Vij, R. Korlacki, G. H. Mehl, and T. Meyer, Phys. Rev. Lett. **93**, 237801 (2004).
[28] J. L. Figueirinhas, C. Cruz, D. Filip, G. Feio, A. C. Ribeiro, Y. Frere, T. Meyer, and G. H. Mehl, Phys. Rev. Lett. **94**, 107802 (2005).
[29] K. Severing and K. Saalwachter, Phys. Rev. Lett. **92**, 125501 (2004).
[30] E. van den Pol, A. V. Petukhov, D. M. E. Thies-Weesie, D. V. Byelov, and G. J. Vroege, Phys. Rev. Lett. **103**, 258301 (2009).

[31] R. W. Date and G. W. Bruce, J. Am. Chem. Soc. **125**, 9012 (2003).

[32] P. H. J. Kouwer and G. H. Mehl, J. Mater. Chem. **19**, 1564 (2009).

[33] J. H. Lee, T. K. Lim, W. T. Kim, and J. I. Jin, J. Appl. Phys. **101**, 034105 (2007).

[34] K. Van Le, M. Mathews, M. Chambers, J. Harden, Quan Li, H. Takezoe, and A. Jakli, Phys. Rev. E **79**, 030701(R) (2009).

[35] M. Nagaraj, Y. P. Panarin, U. Manna, J. K. Vij, C. Keith, and C. Tschierske, Appl. Phys. Lett. **96**, 011106 (2010).

[36] N. Vaupotic, J. Szydlowska, M. Salamonczyk, A. Kovarova, J. Svoboda, M. Osipov, D. Pociecha, and E. Gorecka, Phys. Rev. E **80**, 030701(R) (2009).

[37] T. Ostapenko, C. Zhang, S. N. Sprunt, A. Jakli, and J. T. Gleeson, Phys. Rev. E. **84**, 021705 (2011).

[38] B. Kamala Latha, R. Jose, K. P. N. Murthy, and V. S. S. Sastry, Phys. Rev. E **89**, 050501(R) (2014).

[39] G. De Matteis and S. Romano, Phys. Rev. E **78**, 021702 (2008).

[40] N. Metropolis, A. W. Rosenbluth, M. N. Rosenbluth, A. H. Teller, and E. Teller, J. Chem. Phys. **21**, 1087 (1953).

[41] F. Wang and D. P. Landau, Phys. Rev. Lett. **86**, 2050 (2001); Phys. Rev. E **64**, 056101 (2001).

[42] C. Zhou, T. C. Schulthess, S. Torbrugge, and D. P. Landau, Phys. Rev. Lett. **96**, 120201 (2006).

[43] D. Jayasri, Ph.D. thesis, University of Hyderabad, India, 2009.

[44] S. Romano, Physica A **337**, 505 (2004).

[45] D. P. Landau and K. Binder, *A Guide to Monte Carlo Simulations in Statistical Physics*, 2nd ed. (Cambridge University Press, Cambridge, 2005).

[46] K. P. N. Murthy, *Monte Carlo Methods in Statistical Physics* (Universities Press, India, 2004).

[47] N. Rathore, T. A. Knotts, and J. J. de Pablo, Biophys. J. **85**, 3963 (2003).

[48] D. T. Seaton, T. Wust, and D. P. Landau, Phys. Rev. E **81**, 011802 (2010).

[49] P. Singh, S. K. Sarkar, and P. Bandyopadhyay, Chem. Phys. Lett. **514**, 357 (2011).

[50] P. Poulain, F. Calvo, R. Antoine, M. Broyer, and P. Dugourd, Phys. Rev. E **73**, 056704 (2006).

[51] S. Sinha and S. K. Roy, Phys. Lett. A **373**, 308 (2009).

[52] R. Shekhar, J. K. Whitmer, R. Malshe, J. A. Moreno-Razo, T. F. Roberts, and J. J. de Pablo, J. Chem. Phys. **136**, 234503 (2012).

[53] Y. W. Koh and H. K. Lee, Phys. Rev. E **88**, 053302 (2013).

[54] T. Vogel, Y. W. Li, T. Wust, and D. P. Landau, Phys. Rev. Lett. **110**, 210603 (2013).

[55] K. A. Maerzke, L. Gai, P. T. Cummings, and C. McCabe, J. Phys. Conf. Ser. **487**, 012002 (2014).

[56] Y. L. Xie, P. Chu, Y. L. Wang, J. P. Chen, Z. B. Yan, and J.-M. Liu, Phys. Rev. E **89**, 013311 (2014).

[57] L. Gai, T. Vogel, K. A. Maerzke, C. R. Lacovella, D. P. Landau, P. T. Cummings, and C. McCabe, J. Chem. Phys. **139**, 054505 (2013).

[58] D. Jayasri, V. S. S. Sastry, and K. P. N. Murthy, Phys. Rev. E **72**, 036702 (2005).

[59] P. A. Lebwohl and G. Lasher, Phys. Rev. A **6**, 426 (1972).

[60] B. A. Berg, Comput. Phys. Commun. **153**, 397 (2003).

[61] R. H. Swendsen and J. S. Wang, Phys. Rev. Lett. **58**, 86 (1987).

[62] K. Binder, Z. Phys. B **43**, 119 (1981); Phys. Rev. Lett. **47**, 693 (1981).

[63] R. J. Low, Eur. J. Phys. **23**, 111 (2002).